Application of Junction Capacitance Measurements to the Characterization of Solar Cells

Federico Recart, *Member, IEEE,* and Andrés Cuevas, *Senior Member, IEEE*

***Abstract*—The quasi-static capacitance–voltage (*C–V*) technique measures the dependence of junction capacitance on the bias voltage by applying a slow, reverse-bias voltage ramp to the solar cell in the dark, using simple circuitry. The resulting *C–V* curves contain information on the junction area and base dopant concentration, as well as their built-in potential. However, in the case of solar cells made on low to medium resistivity substrates and having thick emitters, the emitter dopant profile has to be taken into account. A simple method can then be used to model the complete *C–V* curves, which, if the base doping is known, permits one to estimate the emitter doping profile.**

To illustrate the method experimentally, several silicon solar cells with different base resistivities have been measured. They comprise a wide range of areas, surface faceting conditions and emitter doping profiles. The analysis of the quasi-static capacitance characteristics of the flat surface cells resulted in good agreement with independent data for the wafer resistivity and the emitter doping profile. The capacitance in the case of textured surfaces is a function of the effective junction area, which is otherwise difficult to measure, and is essential to understand the emitter and space charge region recombination currents. The results indicate that the effective area of the junction is not as large as the area of the textured surface.

***Index Terms*—Capacitance, photovoltaic cells, space charge region (SCR).**

I. Introduction

THE capacitances present in semiconductor devices are usually a function of relevant physical parameters and their operating conditions, and are relatively easy to measure. As a result, several techniques have been developed historically to characterize, from such measurements, the device's geometry, component materials and interfaces. A number of relatively common techniques are based on capacitive measurements [1], which are very often presented in the form of capacitance–voltage (*C–V*) characteristics.

One of the classic applications of *C–V* curves is the extraction of the dopant concentration of MOS, Schottky diodes and p-n junctions [2]. The capacitance associated with the space charge region (SCR) of the latter is a function of the bias-voltage, the permittivity of the semiconductor, the area of the device, the built-in potential (barrier height in the case of Schottky) and the semiconductor doping profiles. As the permittivity of the material and area of the junction are usually known or can be determined by other methods, the *C–V* curve may be used to obtain the built-in potential and doping profiles. This basic idea has been extended to nonmetallized, nonjunction devices by means of temporary mercury contacts or electrolyte probes, which have been combined with a controlled etch in the powerful electrochemical *C–V* (ECV) technique [3].

The measurement of *C–V* curves of p-n and Schottky junctions is usually performed biasing the device at increasing voltages in a stepped sequence and superimposing a small ac voltage of frequencies ranging from 1 kHz to 1 MHz. This is a well-established method, which leads to the so-called high-frequency (HF) *C–V* data. Specific, and usually expensive, equipment is available for these purposes, which may include among its features a rough analysis of the data for the extraction of the doping profile in the lowly doped side of the diode [4], [5] from the assumption of an abrupt asymmetric junction. Another possibility is the measurement of the capacitance in quasi-steady-state (QSS) conditions. This technique leads to the low-frequency (LF) *C–V* curve, whose comparison with the HF *C–V* is extensively used for the characterization of the dielectric layer in MOS structures. Because of the distinct response-time of the different kinds of charges present in the interface, the differences between the LF and HF curves can provide information on interface states, oxide trapped charges and fixed and mobile charges. Intense research on these topics over the years has led to several methods for the extraction of the *C–V* curve in quasi-static conditions [6]–[10], but their application has, in general, remained restricted to MOS.

The intrinsic simplicity of the QSS philosophy, which lies in the convenience of the data acquisition, performed usually in one-hit using quite simple circuitry, facilitates its use in all kinds of applications. In particular, the widespread use of QSS techniques in the case of photovoltaics [11], [12] is an extra motivation for the application of QSS *C–V* techniques to the characterization of solar cells, some of which are explored in this paper.

II. Theory

A. Transient Model for Solar Cells Under Dynamic Conditions

In diodes and solar cells under dynamic conditions, the charge control model points out the existence of two main capacitive components: the capacitance of the neutral regions and that of the space charge region [13]. In medium and high injections

Manuscript received June 24, 2005; revised October 26, 2005. This work was supported by the Australian Research Council. The work of F. Recart at the Australian National University was supported by a Fellowship from the Basque Government's "Programas de Perfeccionamiento y Movilidad de Personal Investigador." The review of this paper was arranged by Editor P. Panayotatos.

F. Recart is with the Australian National University, Canberra, ACT 0200, Australia, on leave from the Instituto de Tecnología Microelectrónica/ Teknologia Mikroelektronikoaren Institutua (UPV/EHU), Bilbao 48013, Spain (e-mail: federico.recart@ehu.es).

A. Cuevas is with the Department of Engineering, The Australian National University, Canberra, ACT 0200, Australia (e-mail: andres.cuevas@anu.edu.au).

Digital Object Identifier 10.1109/TED.2006.870846

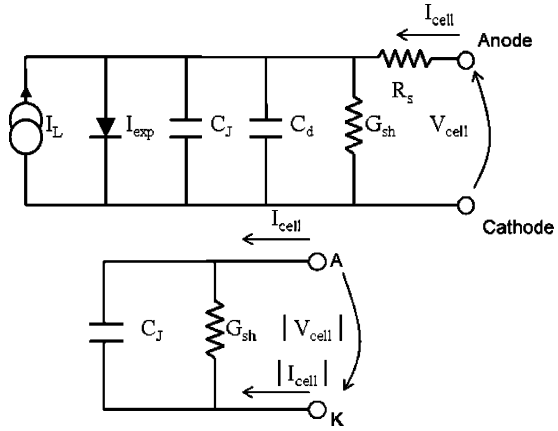

Fig. 1. (Top) Equivalent circuit of a solar cell at moderate frequencies in forward bias, and (bottom) simplified model for a reverse-biased solar cell in the dark.

levels, which usually include the vicinity of the maximum power point, the capacitive inertia of solar cells is dominated by the charge of the excess carriers in the bulk, whose effect has been described in the generalizations of the QSSPC and QSS-$V_{\rm oc}$ methods by Nagel *et al.* [14] and Kerr *et al.* [15], respectively.

However, at low injection levels, and this is the case of cells under reverse or slightly forward bias, the junction capacitance is predominant and has distorting effects in QSS voltage measurements [16]. Therefore, the characterization of the junction capacitance is more necessary, and more easily performed, under very low injection conditions.

If the changes in the voltage are not too fast, a solar cell can be modeled using the circuit shown on the top side of Fig. 1, where I_L represents the photogenerated current; I_{exp} stands for the current predicted by a two exponential model of the diode; C_J and C_d are the capacitances related to the carrier change in the space charge region and in the neutral regions respectively; $G_{\rm sh}$ stands for the leakage currents and R_S lumps together the series resistance effects. But if the cell is in the dark and reverse-biased, there is no photogeneration $(I_L = 0)$ and the currents due to the two-exponential model are negligible $(I_{exp} \sim 0)$. In addition, there are very few minority carriers in the neutral regions $(C_d \sim 0)$ and, for low reverse currents, the voltage drop in the series resistance is usually very small. In these conditions the model simplifies to that shown on the bottom side of the same Fig. 1.

In this quasi-steady-state case, the relationship between the voltage and the current can be written as

$$i_{\rm cell} = G_{\rm sh} \cdot v_{\rm cell} + C_J \cdot \frac{dv_{\rm cell}}{dt} \Rightarrow C_J = \frac{i_{\rm cell} - G_{\rm sh} \cdot v_{\rm cell}}{\frac{dv_{\rm cell}}{dt}} \quad (1)$$

This formula leads to a capacitance value for every instantaneous value of the applied voltage, and it represents the basic theoretical principle of the QSS-CJ method.

B. Junction Capacitance Model

The space-charge-region capacitance of a p-n junction shows a strong dependence on the reverse voltage, which is usually modeled by [17]

$$C_J = \varepsilon_0 \varepsilon_r \cdot \frac{A}{w_{\rm SCR}} = C_{J0} \cdot \left(1 - \frac{V_{\rm cell}}{V_{\rm intercept}}\right)^{-\frac{1}{m}} \quad (2)$$

where ε_0 is the permittivity of the vacuum (88.54 fF/cm); ε_r is the relative dielectric constant of the material (in the case of silicon, $\varepsilon_r = 11.8$); A is the area of the device; $w_{\rm SCR}$ is the width of the space charge region; C_{J0} is the capacitance of the junction in equilibrium; and $V_{\rm intercept}$ is an auxiliary voltage, which corresponds to the extrapolated value for $C_J^{-1} = 0$ and is usually assumed equal to $V_{\rm bi}$, the built-in potential. The factor m depends on the shape of the dopant profile at the junction and equals 2 for an abrupt junction, which will be used here as the basis for a first-order approach because it is usually a good approximation in the case of solar cells. Note also that (2) is valid only under reverse bias or low forward voltages and that high injection operation requires other models [18], [19].

Abrupt Asymmetrical p-n Junctions: The equilibrium value of the junction capacitance is given by [17]

$$C_{J0} = \varepsilon_0 \varepsilon_r \cdot \frac{A}{w_{\rm SCREQ}} = \frac{\varepsilon_0 \varepsilon_r \cdot A}{\sqrt{\frac{2\varepsilon_0 \varepsilon_r}{q} \cdot \left(\frac{1}{N_{\rm Bulk}} + \frac{1}{N_{\rm Emitter}}\right) \cdot V_{bi}}} \quad (3)$$

where $w_{\rm SCR}\, EQ$ is the width of the space charge region in equilibrium, $q = 1.602 \times 10^{-19}\ C$, and $N_{\rm Bulk}$ and $N_{\rm Emitter}$ are the doping concentrations in the bulk and the emitter, respectively.

Considering the usual doping asymmetry of the typical silicon solar cells $(N_{\rm Bulk} \ll N_{\rm Emitter})$

$$C_{J0} \approx A \cdot \sqrt{\frac{q \cdot \varepsilon_0 \varepsilon_r \cdot N_{\rm Bulk}}{2 \cdot V_{\rm bi.}}} \quad (4)$$

From (2), with $m = 2$, and (4), it is easily proven that the slope of the $C_J^{-2} - V$ curve and the doping concentration of the bulk are related by

$$-\frac{d\left(\frac{1}{C_J^2}\right)}{dV_{\rm cell}} = \frac{2}{q\varepsilon_0 \varepsilon_{\rm rmat} \cdot A^2 \cdot N_{\rm Bulk}}. \quad (5)$$

So, the bulk doping concentration can be extracted from the slope of the $C_{\rm J}^{-2} - V$ characteristic, and the intercept with $1/C_J = 0$ gives the built-in potential. The uncertainty of the geometrical method used for the extraction of the intercept is high and, in addition, the value of the intercept is per se shifted from the real built-in potential [20], so the technique can only estimate $V_{\rm bi}$ very roughly. Despite this, the method may be useful when the objective is to get an approximate value or to characterize the junction in the case of structures or materials not as well known as crystalline silicon [21].

If (5) is applied to every "bias" voltage, the doping concentration at the edge of the space charge region can be obtained [1]. And as the junction is one-sided, the distance from this point to the metallurgical junction is the width of the SCR, which is directly related to the capacitance from (2). As a result, these two equations allow for obtaining the doping profile near the metallurgical junction and are the basis for the common *C–V* profiling techniques. When the method is applied to solar cells which fulfill the abrupt-junction conditions, nonuniform bulk doping profiles can be characterized.

The main limitations of applying this method for the profiling are the maximum depletion that can be achieved by applying a reverse bias before entering in the junction breakdown region, the presence of large leakage currents, and the weakness of the

abrupt junction hypothesis. These issues are solved in the ECV technique, which only measures the surface concentration of a semiconductor-electrolyte Schottky junction and performs a controlled etching of the semiconductor surface to achieve the profiling, with the only remaining limitation being the minimum spatial resolution, given by the Debye length [3].

p-n Junctions With Gaussian Emitters: When *C–V* curves are used to extract the dopant concentration of a uniform bulk region, the calculation of the average slope of the $1/C_J^2 - V$ characteristic, and the use of (4), usually lead to good results for high and medium resistivities, even with moderately graded emitters. Nevertheless, as the analysis is strictly valid only for abrupt and asymmetric junctions, it fails when applied to low resistivity substrates, particularly if thick, nonabrupt, emitters are present.

The analytical study of curves of Gaussian or exponential emitter junctions is quite complex [22], [23] and to explore the issue of nonuniform emitters, numerical methods are more convenient. In addition, when both emitter and bulk must be considered, there will be several possible combinations of emitter-profile and bulk doping for every *C–V* characteristic [24].

To investigate this, a general-purpose mathematical program has been used to calculate *C–V* curves for Gaussian emitters and uniform bulks on the basis of the depletion approximation and using the emitter profile defined by

$$N_E(x) = N_{\rm ES} \times \exp\left[-\left(\frac{x}{x_G}\right)^2\right] \tag{6}$$

and the bulk doping concentration (N_B) as inputs. It starts from the assumption of an initial width of the SCR toward the emitter and calculates the corresponding charge and the required width of the depleted region toward the base to ensure global charge neutrality. The electrostatic potential and the voltage are then obtained by integrating twice the charge; the capacitance can now be obtained from (2), where all the parameters are known. By applying this simple process for a range of SCR widths, the *C–V* curve is reconstructed. The *C–V* characteristics predicted by this numerical method are in excellent agreement with PC1D [25] simulations for a range of bulk concentrations from 10^{13} to 10^{18} cm^{-3} and for Gaussian emitters with a wide range of x_G characteristic lengths (including $x_G = 0.01$ μm, i.e., the abrupt case).

Fig. 2 shows (open symbols) *C–V* curves simulated by PC1D for a cell with a low resistivity (0.1 $\Omega \cdot$ cm, $N_B = 2.34 \times 10^{17}$ cm^{-3}), and emitters with fixed surface concentration ($N_{\rm ES} = 10^{19}$ cm^{-3}) but several different grades of abruptness, defined by their Gaussian characteristic lengths. The corresponding numerical fits on the basis of (2) and (4) (represented by the filled symbols of Fig. 2) show that, for thick emitters, the abrupt-junction approximation can not provide a good fit to the whole curve and, in addition, it leads to an underestimation of the dopant concentration in the base. The two nonabrupt junctions shown in Fig. 2 (for $x_G = 0.4$ and 1.2 μm) have increasingly wider space charge regions and, subsequently, smaller capacitances, compared to the abrupt junction case ($x_G = 0.01$ μm). To achieve a wider depletion region, the abrupt-junction model needs to decrease the base dopant density, leading to an erroneous determination

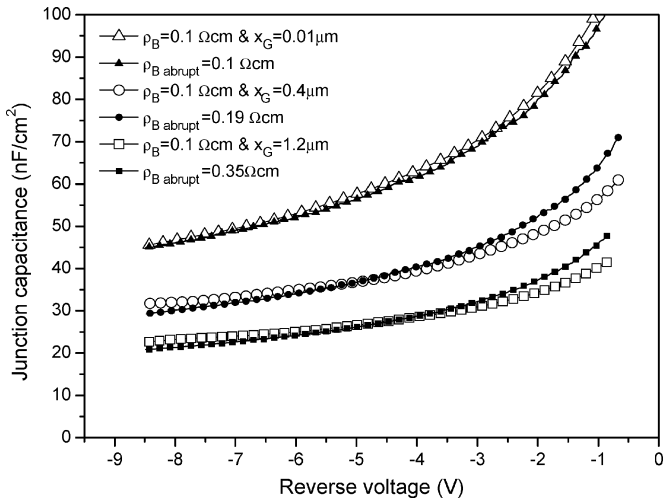

Fig. 2. Simulated *C–V* curves for cells made on 0.1 Ωcm substrates with different Gaussian emitters (open symbols) and best fits on the basis of the abrupt junction approximation (filled symbols). The numerical reconstructions described in the text are fully coincident with the PC1D simulations.

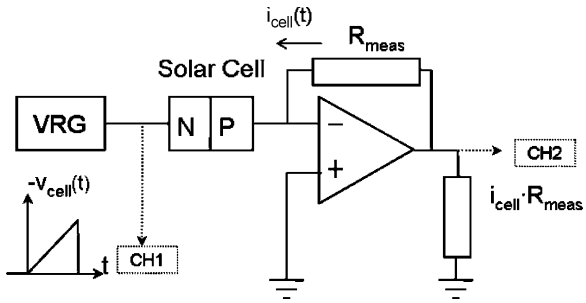

Fig. 3. Block diagram for the measurement of the QSS junction capacitance.

of its value. In the case of the thickest emitter ($x_G = 1.2$ μm, corresponding to a junction depth of $x_{\rm J} = 2.4$ μm) the error in the resistivity would be 240% ($\rho_{\rm sample} = 0.1$ $\Omega \cdot$ cm, $\rho_{\rm abrupt\ fit} = 0.34\ \Omega \cdot$ cm). On the other hand, the *C–V* curves reconstructed by the procedure described above match perfectly the PC1D simulations (the numerical Gaussian fits have been omitted in Fig. 2 to enhance its clarity).

III. Experimental

A. Measuring the Quasi-Static Capacitance

The circuit for the measurement of the QSS junction capacitance (see Fig. 3) consists of a voltage ramp (with a rather slow, adjustable slope) and an operational amplifier. It is based in a design used by Kuhn [6] for the measurement of the quasi-static capacitance of MOS structures. The negative feedback of the operational amplifier forces both the reverse voltage in the cell to be equal to the ramp and the appearance of a signal proportional to the cell current in the output of the circuit. The reliability of the system has been tested with discrete capacitors ranging from 150 pF to 10 μF, obtaining in all the cases the nominal values within errors smaller than 5%.

When applying the method to solar cells, special care must be taken when selecting the slope of the ramp: if the selected ramp is too slow, the leakage current can be dominant and mask the capacitive current; on the other hand, fast ramps applied to cells

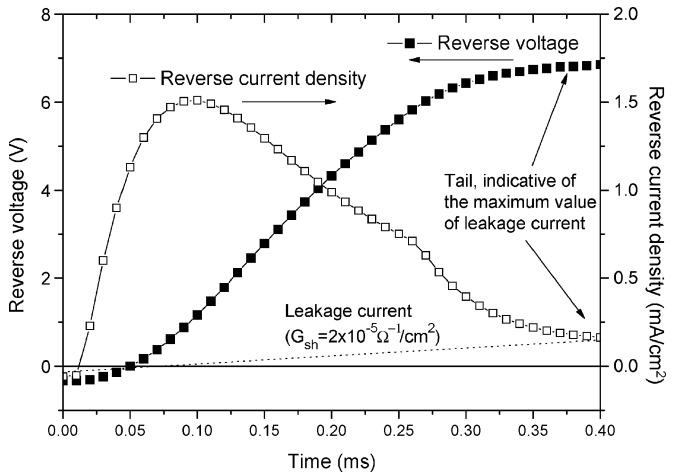

Fig. 4. Experimental current (open squares) and voltage (filled squares) waveforms for a silicon solar cell (p-type, area $= 4$ cm^2) measured by applying a voltage ramp of 25 V/ms approximately.

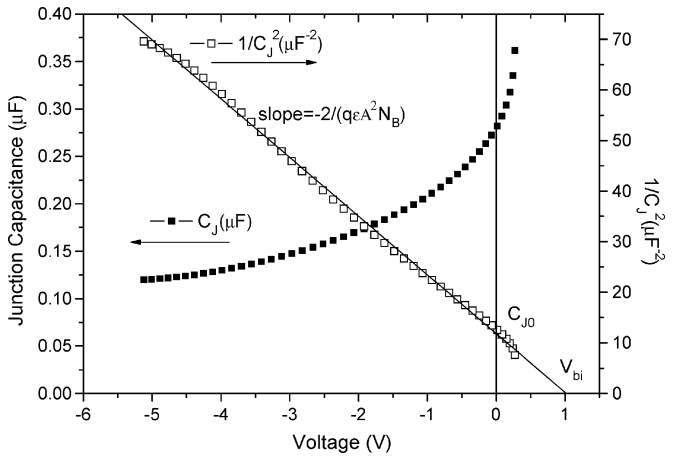

Fig. 5. Experimental C–V curve (filled squares) and $C_J^{-2} - V$ data (open squares) and fitted curve (line).

with large capacitances (high dopant concentrations) can lead to a saturation of the current channel. Slopes of 10 to 100 V/ms applied during 100 μs-1 ms are usually appropriate. Fig. 4 shows a typical waveform, obtained in this case with a voltage ramp of 25 V/ms. In response to the changing voltage, a strong reverse current is rapidly established, reaching a maximum and declining thereafter as the voltage ramp tapers off. The final part of the current waveform is dominated by the shunt resistance of the device.

Although the main information is contained in the central part of the measured interval, the final tail is a good starting point for the analysis, because the voltage is constant and the current, free of capacitive effects, gives a good measure of the leakage current. It may be modeled, in the case of Fig. 4, by a shunt of $G_{\rm sh} = 2 \times 10^{-5}$ S/cm^2. It is observed that the leakages have a minor weight in the current and, applying (1), the junction capacitance can be accurately determined for every voltage. As a guideline, although the leakage component can be subtracted, if it contributes more than 50% of the total current, it is recommended to acquire a new waveform using a faster ramp.

The same circuit can also be used, applying slower voltage ramps, for a more accurate determination of $G_{\rm sh}$. These auxiliary curves may be especially useful for the analysis of leakage currents that are nonlinear in the reverse bias region. Such nonlinear behavior has been shown to be explainable by the impact ionization mechanism [26]. The resistive and capacitive components may also be distinctly characterized by applying a triangular voltage waveform that provides two points for every voltage with the same leakage current but different capacitive currents [8]. As an alternative technique, leakage currents can be studied using infrared thermography techniques [27], [28], which have the added attraction of producing a two-dimensional map of localized shunts.

The capacitance data of solar cells measured in this way have been successfully checked by comparison to the values obtained with a commercial LCR (inductance, capacitance, resistance) impedance meter for a set of voltages and frequencies: the QSS C–V curves matched perfectly the values obtained at low frequencies (100 Hz) by the commercial equipment using the ac small signal method.

TABLE I
SUMMARY OF APPROXIMATE RESULTS FOR SEVERAL CRYSTALLINE SILICON SOLAR CELLS, OBTAINED WITH THE LINEAR MODEL (ABRUPT JUNCTION APPROXIMATION)

Cell	Type	G_{sh} ($k\Omega^{-1}$)	ρ_{nom} (Ωcm)	ρ_{abrupt} (Ωcm)	Emitter	Surface
Ma6	N	0.002	110	106	Very thick	Textured
12E	P	0.01	21	19.6	Thick	Textured
88A12	P	0.01	21	19.3	Thick	Polished
F7B	P	0.001	1	0.81	Medium	Textured
9E	P	0.058	0.33	0.31	Thick	Textured
88AC7	P	0.1	0.33	0.52	Thick	Polished
2E	P	0.025	0.11	0.17	Thick	Polished
88AC3	P	0.8	0.11	0.27	Very thick	Polished

It should be noted that the analysis methods and the applications described in this paper also apply to measurements obtained with commercial C–V systems. Such systems usually offer the added possibility of making high frequency measurements, which are particularly useful for MOS devices. An extended analysis focusing on the frequency response of the resistive and capacitive components of the complex impedance has recently been shown to be useful for the investigation of thin film solar cells [21].

B. Preliminary Analysis of the C–V Curves, Based on the Abrupt Junction Hypothesis

As discussed above, the analysis of the $C_J^{-2} - V$ curve based on the approximation of having an abrupt junction is usually a good approach. The average slope is directly translated into a preliminary value for the bulk doping concentration and the intercept with $1/C_J = 0$ estimates the built-in voltage. Fig. 5 shows the measured curves and analytical fits for a representative silicon solar cell. The values calculated from the slope and the intercept are in this case $N_{\rm Bfit\ abrupt} = 6.4 \times 10^{16}$ cm^{-3} and $V_{\rm intercept} = 1.02$ V.

Table I summarizes some indicative results obtained in this way for a wide range of silicon solar cells. It also includes details on the junction depth and the faceting (or not) of the surface.

The agreement between the doping density obtained from the C–V measurements and the nominal wafer resistivity is

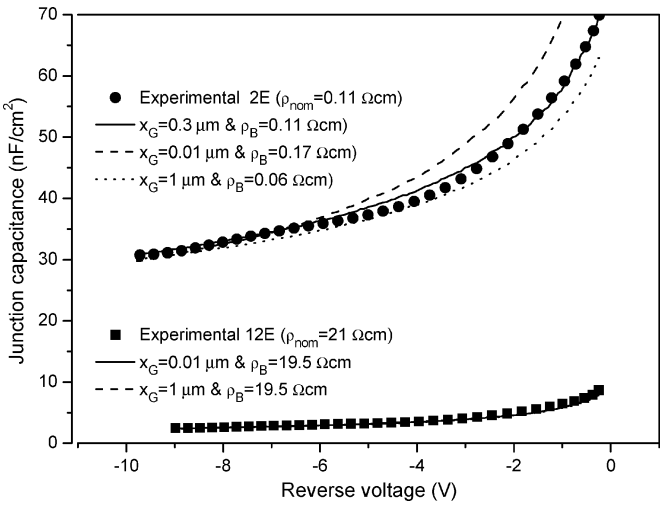

Fig. 6. Experimental *C–V* characteristics (symbols) and possible fits (lines) using Gaussian emitter dopant profiles for cells 2E (above) and 12E (below). The emitter surface concentration was maintained constant, $N_{\rm ES} = 10^{19}$ cm^{-3}. In the case of cell 12E the simulated curves for the two extreme Gaussian profile cases overlap.

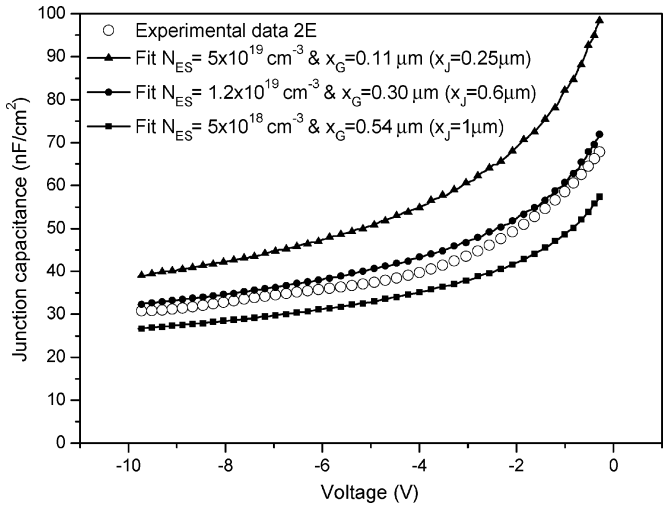

Fig. 7. Experimental *C–V* curve for cell 2E and modeled curves with fixed $\rho(0.1\ \Omega \cdot \text{cm})$ and three emitters.

very good (within 10%) for low bulk doping concentrations, because this improves the accuracy of the one-sided abrupt junction hypothesis (especially if thin emitters are present). For low resistivities, the error using the abrupt-junction approximation increases (up to 150% in some cases), as anticipated in Section II. This effect can be corrected for if the shape of the emitter is approximately known. Alternatively, if the resistivity is known, this apparent disadvantage can be turned into a method for the characterization of the emitter, as explained in the next section.

In some cases, a difference between polished and textured cells can also be observed, which will be discussed in Section III-D.

C. Determining the Approximate Emitter Doping Profile

The cells made on low resistivity substrates (last rows of Table I) reveal the weakness of the abrupt junction approximation. The analysis of their *C–V* curves has to take into account the profile of the emitter, which here, for simplicity and wide applicability, will be assumed to be Gaussian. There are, in principle, different combinations of emitter and base doping concentrations leading to similar characteristics [22] and, so, the analysis of the *C–V* curves with this complete model (assuming uniform bulk concentrations) results in several possible solutions.

Fig. 6 shows three possible fits for cells 2E (upper curves) and 12E (lower curves). The surface concentration has been maintained equal to $N_{\rm ES} = 10^{19}$ cm^{-3}. These results indicate that the *C–V* curve of the high resistivity wafer (12E) is insensitive to changes in the emitter profile and the nominal bulk doping ($N_{\rm Bnominal} = 6.44 \times 10^{14}$ cm^{-3}) is obtained in all cases, with an error smaller than 10%. On the contrary, the fits for 2E ($\rho_{\rm Bnominal} = 0.11\,\Omega \cdot$cm, $N_{\rm Bnominal} = 2.06 \times 10^{17}$ cm^{-3}) are very sensitive on the emitter thickness and can only conclude that the doping would be between 0.344 $\Omega \cdot$ cm (if an abrupt emitter is assumed) and 0.058 $\Omega \cdot$ cm (if a Gaussian emitter with $x_G = 1.0\ \mu$m, which corresponds to a junction depth $x_J = 1.4\ \mu$m, is used). The shape of the *C–V* curve indicates that 0.11 $\Omega \cdot$cm ($N_{\rm B} = 2.1 \times 10^{17}$ cm^{-3}) and $x_G = 0.3\ \mu$m is the most probable combination but, if one assumes a 5% error for the capacitance, this best fit must be understood only as indicative. In summary, in the case of low resistivity cells, it is necessary to know the approximate shape of the emitter or, at least, know if it is thin ($< 0.5\ \mu$m), medium or thick ($> 1\ \mu$m).

TABLE II
SUMMARY OF RESULTS FOR SOME CRYSTALLINE SILICON SOLAR CELLS, WITH THE COMPLETE MODEL

Cell	Type	G_{sh} (kΩ^{-1})	ρ_{nom} (Ωcm)	$\rho_{fit\ abrupt}$ (Ωcm)	Emitter[a] (using ρ_{nom} as input)
Ma6	N	0.002	110	106	Insensitive
12E	P	0.01	21	19.6	Insensitive
88AC12	P	0.01	21	19.6	Insensitive
88AC7	P	0.1	0.33	0.52	N_{ES}=10^{19} cm^{-3} x_J=0.6μm
2E	P	0.025	0.11	0.17	N_{ES}=1.2x10^{19} cm^{-3} x_J=0.6μm
88AC3	P	0.8	0.11	0.27	N_{ES}=2x10^{19} cm^{-3} x_J=1.8μm

Alternatively, if the bulk resistivity and the sheet resistance are known (in the case of cell 2E, $\rho_{\rm Bulk\ nominal} = 0.11\ \Omega \cdot$cm and $R_{\rm Sheet\ emitter} = 140\ \Omega/\square$) the *C–V* curve can be used to characterize the emitter. Fig. 7 shows a set of characteristics reconstructed on this basis. The conclusion is that the most probable emitter (if Gaussian) has a surface concentration of $N_{\rm ES} = 1.2 \times 10^{19}$ cm^{-3} and a characteristic depth of $x_G = 0.3\ \mu$m (a resulting junction depth of $x_J = 0.6\ \mu$m). The same procedure can be applied to cell 88AC3 ($\rho_{\rm Bulk\ nominal} = 0.11\ \Omega \cdot$cm, and $R_{\rm Sheet\ emitter} = 36\ \Omega/\square$), obtaining in this case a much thicker emitter, with $N_{\rm ES} = 2 \times 10^{19}$ cm^{-3} and a characteristic depth of $x_G = 0.83\ \mu$m ($x_J = 1.77\ \mu$m). These results agree very well with the profiles that were obtained for these emitters by incremental resistivity and hall effect measurements [29]. Table II shows a summary of the results, stating the opportunity offered by this technique for the rough profiling of Gaussian emitters using low resistivity substrates.

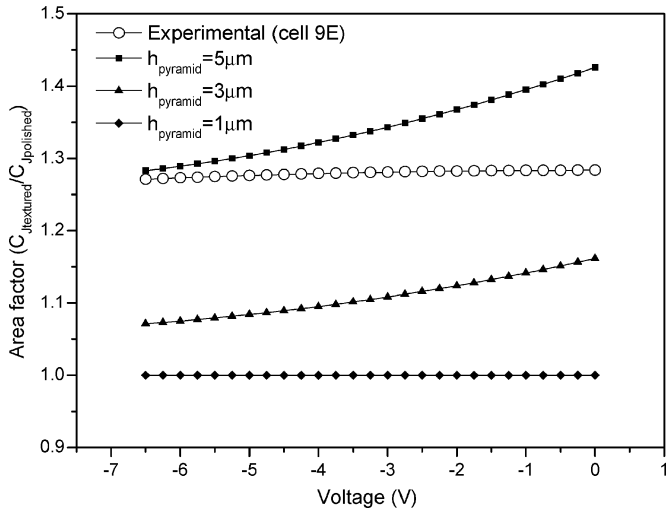

Fig. 8. Experimental junction area factor of cell 9E and simulations (PC1D) of the structure ($\rho_B = 0.33\ \Omega$cm, $N_{\rm ES} = 10^{19}$ cm^{-3}, $x_G = 0.3\ \mu$m) using a texturization with three pyramid sizes.

D. Effect of Surface Faceting

Most monocrystalline solar cells have textured front surfaces to maximize the absorption of the incident light. This increases not only the effective area of the surface and the recombination in the underlying emitter [30], but also the geometry and recombining properties of the space charge region. The effective area of such surfaces is difficult to evaluate and it is usually estimated using geometrical models [25]. To measure it experimentally, the *C–V* characterization of parallel textured MOS structures can be used [31], and this may, in addition, lead to a better knowledge of the interface. In this context, the *C–V* characteristic of solar cells is a natural and convenient way of exploring the effective area of the depleted junction and it provides information about this important, and often ignored, region.

The increased junction area caused by the texturization has its maximum effect at the surface and it is expected to fade toward the bulk quite rapidly. The model used by PC1D, for instance [25], accounts for the cross section area of the device by means of a Gaussian function with a characteristic length equal to one-sixth of the pyramid size. This means that the effective area of the junction is a function of the texturization, but also of the thickness of the emitter, the base doping and the applied voltage, because all of them determine the depth of the SCR edge. The simulations of the effect are very sensitive to the inputs and to the actual mathematical model used.

In practice, it is possible to take advantage of the direct relationship between junction area and capacitance to determine an effective area factor, which can be defined as the ratio between the experimental junction capacitance of the textured solar cell and the modeled value that would correspond to a similar cell with a flat surface. This requires the knowledge of the base resistivity and approximate emitter shape, which can be determined as described in previous sections. The area factor $F_{\rm Text}$ is

$$F_{\rm Text} = \frac{C_{\rm Experimental\ textured}}{C_{\rm Modeled\ flat\cdot}} \tag{7}$$

This expression gives an effective junction area for every voltage, but the most meaningful value corresponds to low reverse voltages, near equilibrium, because they are closer to the effective area in the usual forward bias operating conditions.

TABLE III
SUMMARY OF JUNCTION AREA FACTORS OF THE TEXTURED CELLS SHOWN IN TABLE I (CALCULATED FOR SMALL REVERSE VOLTAGES)

Cell	Type	$\rho_{\rm nom}$ (Ωcm)	$\rho_{\rm fit\ abrupt}$ (Ωcm)	Emitter	Area factor
Ma6	N	110	106	Insensitive	~1
12E	P	21	19.6	Insensitive	~1
F7B	P	1	0.81	Not very sensitive	1.35
9E	P	0.33	0.31	$N_{ES}=10^{19}$ cm^{-3} $x_J=0.69\mu$m[a]	1.25

[a] *Emitter profile determined from a similar polished cell, 88AC7*

Fig. 8 shows the dependence of the area factor on the reverse voltage according to PC1D simulations for three different pyramid sizes. Note that a pyramid height of 1 μm has practically no effect on the junction area ($F_{\rm Text} \sim 1$) and also that the highest area factor in this example ($F_{\rm Text} \sim 1.45$) is still well below the ratio of geometrical ratio of 1.7 that would apply to the outer pyramidal surface. In addition, Fig. 8 shows the experimental results obtained for a solar cell (sample 9E) having the same base resistivity (0.33 ohm.cm) assumed for the PC1D simulations and a similar Gaussian emitter profile. By comparing the experimental and modeled curves, especially at large reverse bias, one can conclude the average size of the pyramids is approximately 5 μm. Nevertheless, there is a notable disagreement for lower reverse voltages. This can be attributed to the fact that the experimental texturization process (a chemical etch in a mix of NaOH and isopropanol) typically results in a random distribution of pyramid sizes. The smaller pyramids dominate at low reverse voltages and tend to reduce the area factor.

Table III shows the experimental effective factor area obtained for the textured cells of Table I.

The values for high resitivities are close to one, because the SCR is so wide that the effect of texturization is negligible. For medium (1 $\Omega \cdot$ cm) and low resitivities (0.33 $\Omega \cdot$ cm), the SCR is narrower and the effective area of the junction increases by 25% and 35% respectively, which helps to explain the higher recombination currents observed in the SCR of textured silicon solar cells, especially when large pyramids are present [32].

The technique could be applied to nonconventional solar cells, where the junction area may be more difficult to determine, such as emitters with double diffusions, such as the buried contact solar cell. It can also be used to study nongeometrical texturing methods, such as the acidic texturing used for mc-Si solar cells.

IV. CONCLUSION

The QSS approach offers a good opportunity for measuring the junction capacitance of solar cells. By using simple circuitry, *C–V* characteristics can be obtained in a convenient way and with good accuracy. These *C–V* curves contain information about the doping concentration, the built-in voltage, the emitter profile and the junction topography.

The first-order analysis of the experimental *C–V* curves based on the abrupt junction hypothesis shows that this approximation can be applied to solar cells made on high and medium resistivity wafers with thin emitters. On the other hand, the analysis

of cells with low resistivity base regions and thick emitters requires further attention. In this work, a simple, iterative method has been proposed for the reconstruction of *C–V* curves for the representative case of Gaussian emitters, and it has been verified both by PC1D simulations and experimentally. The dependence of the junction capacitance of low resistivity cells on the emitter dopant profile allows for an approximate characterization of the latter in a very simple and nondestructive way.

The case of textured cells has also been studied, showing that the effective junction area is not as large as the geometrical ratio between the textured and flat surfaces. The effective junction area factor, whose knowledge is relevant to understanding the recombination in the SCR region, has been experimentally measured and numerically simulated, leading to different values depending on the bulk doping concentration, emitter profile and texturing geometry.

In addition to the specific applications described above, the determination of the junction capacitance, facilitated by the simple technique developed here, is essential to understand the behavior of solar cells in dynamic, time-dependent conditions [16].

REFERENCES

[1] D. K. Schroder, *Semiconductor Material and Device Characterization*, 2nd ed. New York: Wiley, 1998, pp. 62–99.

[2] J. Hilibrand and R. D. Gold, "Determination of the impurity distribution in junction diodes from capacitance-voltage measurements," *RCA Rev.*, vol. 21, pp. 242–252, 1960.

[3] P. Blood, "Capacitance–voltage profiling and the characterization of III-V semiconductors using electrolyte barriers," *Semicond. Sci. Technol.*, vol. 1, pp. 7–27, 1986.

[4] Analysis of semiconductor capacitance characteristics—Using the HP 4280A 1 MHz C meter/*C–V* plotter, Hewlett Packard—Application note 322, 1986.

[5] (2001) Accurate and efficient *C–V* measurements. Agilent Technologies Application note E5250A-3. [Online]Available: www.agilent.com

[6] M. Kuhn, "A quasi-static technique for MOS *C–V* and surface state measurements," *Solid State Electron.*, vol. 13, pp. 873–885, 1970.

[7] W. K. Kapallo and J. P. Walsh, "A current voltage technique for obtaining low-frequency *C–V* characteristics of MOS capacitors," *Appl. Phys. Lett.*, vol. 17, no. 9, pp. 384–386, 1970.

[8] N. J. Chou, "Application of triangular voltage sweep method to mobile charge studies in MOS structures," *J. Electrochem. Soc.*, vol. 118, pp. 601–609, 1971.

[9] Y. T. Yeow, M. R. Boudry, D. R. Lamb, and S. D. Brotherton, "Sources of errors in quasi-static capacitance-voltage determination of the interface state density distribution in the MOS system," *Appl. Phys.*, vol. 10, pp. 83–95, 1977.

[10] T. J. Mego, "Improved quasi-static CV measurement method for MOS," *Rev. Sci. Instr.*, vol. 57, no. 11, pp. 2798–2805, 1986.

[11] R. A. Sinton and A. Cuevas, "Contactless determination of current-voltage characteristics and minority carrier lifetimes in semiconductors from quasi-steady-state photoconductance data," *Appl. Phys. Lett.*, vol. 69, no. 17, pp. 2510–2512, 1996.

[12] ——, "A quasi-steady-state open-circuit voltage method for solar cell characterization," in *Proc. 16th Eur. PVSEC*, 2000, pp. 1152–1155.

[13] H. K. Gummel and H. C. Poon, "An integral charge control model of bipolar transistors," *Bell Syst. Tech. J.*, vol. 49, p. 827, 1970.

[14] H. Nagel, C. Berge, and A. G. Aberle, "Generalized analysis of quasi-steady-state and quasi-transient measurements of carrier lifetimes in semiconductors," *J. Appl. Phys.*, vol. 86, no. 11, pp. 6218–6221, 1999.

[15] M. J. Kerr, A. Cuevas, and R. A. Sinton, "Generalized analysis of quasi-steady-state and transient decay open circuit voltage measurements," *J. Appl. Phys.*, vol. 91, no. 1, pp. 399–404, 2002.

[16] A. Cuevas and F. Recart, "Capacitive effects in quasi-steady-state voltage and lifetime measurements of silicon devices," *J. Appl. Phys.*, vol. 98, no. 7, pp. 4507–4513, 2005.

[17] S. M. Sze, *Semiconductor Devices, Physics and Technology*. New York: Wiley, 1985.

[18] J. J. Liou and F. A. Lindholm, "Capacitance of semiconductor p-n junction space-charge layers: an overview," *Proc. IEEE*, vol. 76, no. 11, pp. 1406–1422, Nov. 1988.

[19] P. Van Halen, "A new semiconductor junction diode space charge layer capacitance model," in *Proc. IEEE Bipolar Circuits Technol. Meeting*, 1988, pp. 168–171.

[20] P. Van Mieghem, "Origin of the difference between the capacitance intercept voltage and the built-in potential," *IEEE Trans. Electron Devices*, vol. 40, no. 12, pp. 2365–2368, Dec. 1993.

[21] A. Straub, R. Gebs, H. Habenicht, S. Trunk, R. A. Bardos, A. B. Sproul, and A. G. Aberle, "Impedance analysis: a powerful method for the determination of the doping concentration and built-in potential of non ideal semiconductor p-n diodes," *J. Appl. Phys.*, vol. 97, no. 8, pp. 3703–3710, 2005.

[22] P. Van Halen, "Characterization of junction capacitance parameters for Gaussian/constant doping profiles," in *Proc. IEEE Symp. Circuits Syst.*, 1989, pp. 852–855.

[23] F. D. Ho, "Simple model for space charge region capacitance of an exponential-constant p-n junction," *Electron. Lett.*, vol. 26, no. 25, pp. 2063–2065, 1990.

[24] D. Salameh and D. Linton, "Study of the relation between doping profile and diode CV characteristics," *IEEE Trans. Microw. Theory Tech.*, vol. 47, no. 4, pp. 506–509, Jul. 1999.

[25] P. Basore, "Numerical modeling of textured silicon solar cells using PC-1D," *IEEE Trans. Electron Devices*, vol. 37, no. 2, pp. 337–343, Feb. 1990.

[26] M. C. Alonso and J. M. Ruiz, "A new model for the characterization of *I–V* curves of silicon solar cells in reverse bias," in *Proc. 19th Eur. PVSEC*, 2004, pp. 2607–2610.

[27] O. Breitenstein, J. P. Rakotoniaina, and M. H. Al Rifai, "Quantitative evaluation of shunts in solar cells by lock-in thermography," *Prog. Photovolt.*, vol. 11, pp. 515–526, 2003.

[28] O. Breitenstein, J. P. Rakotoniaina, M. H. Al Rifai, and M. Werner, "Shunt types in crystalline silicon solar cells," *Prog. Photovolt.*, vol. 12, pp. 529–538, 2004.

[29] A. Cuevas and M. Balbuena, "Thick-emitter silicon solar cells," in *Proc. 20th PVSEC*, 1988, pp. 429–433.

[30] M. J. Kerr, J. Schmidt, A. Cuevas, and J. H. Bultman, "Surface recombination velocity of phosphorus-diffused silicon solar cell emitters passivated with plasma enhanced chemical vapor deposited silicon nitride and thermal silicon oxide," *J. Appl. Phys.*, vol. 89, no. 71, pp. 3821–3826, 2001.

[31] S. Tietun, C. Dong, and C. Rongqiang, "Surface texturing of crystalline silicon and effective area measurement," *Proc. SPIE*, vol. 4086, pp. 116–119, 2000.

[32] F. Hernando, J. R. Gutiírrez, G. Bueno, F. Recart, and V. Rodríguez, "Humps, a surface damage explanation," in *Proc. 2nd World Conf. Exhibition Photovolt. Sol. Energy Conv.*, 1998, pp. 1321–1323.

Federico Recart (M'98) received the M.E. degree in telecommunications in 1994 and the Ph.D. degree in solar cells in 1994 and 2001, respectively, both from the University of the Basque Country, Bilbao, Spain.

His research work, developed since 1993 at the Instituto de Tecnología Microelectrónica/Teknologia Mikroelektronikoaren Institutua, comprises industrial manufacturing technologies, modeling and characterization of silicon solar cells. Since 2003, he holds an Associate Professor appointment at the Department of Electronics and Telecommunications, University of the Basque Country.

Andrés Cuevas (SM'95) received the M. Eng. degree in telecommunications and the Ph.D. degree in 1976 and 1980, respectively, both from the Universidad Politécnica de Madrid, Madrid, Spain.

He has held academic positions at the Universidad Politécnica de Madrid from 1980 to 1993 and at The Australian National University, Canberra, Australia, where he is currently Professor of Electrical Engineering. He has been a Fulbright Scholar at Stanford University and a Visiting Researcher at the universities of Florida and Catalunya, the CNR-Bologna, the ENEA-Portici in Italy, and the Fraunhofer ISE in Freiburg. His contributions to the field of silicon solar cells are described in more than 220 scientific publications, including several patents and book chapters. His broad interests in semiconductor physics and technology have recently focused on novel characterization techniques for electronic materials and devices, the study of fundamental properties of silicon, the passivation of its surfaces by means of silicon nitride, and the advancement of multicrystalline silicon solar cells.